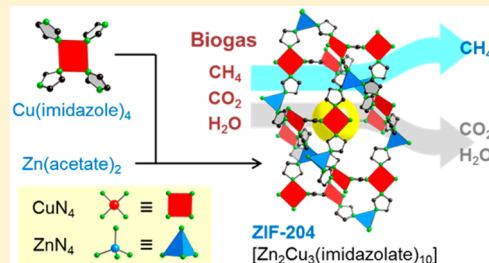


Mixed-Metal Zeolitic Imidazolate Frameworks and their Selective Capture of Wet Carbon Dioxide over Methane

Nhung T. T. Nguyen,^{†,‡,#} Tien N. H. Lo,^{†,#} Jaheon Kim,[§] Huong T. D. Nguyen,[†] Toan B. Le,^{†,‡} Kyle E. Cordova,^{*,†,||} and Hiroyasu Furukawa^{*,†,||}[†]Faculty of Chemistry, University of Science, Vietnam National University-Ho Chi Minh City, Ho Chi Minh City 721337, Vietnam[‡]Department of Chemistry, School of Education, Can Tho University, Can Tho City 721337, Vietnam[§]Department of Chemistry, Soongsil University, 369 Sangdo-Ro, Dongjak-Gu, Seoul 156-743, Republic of Korea[†]Department of Chemistry, University of California-Berkeley; Materials Sciences Division, Lawrence Berkeley National Laboratory; and Berkeley Global Science Institute, Berkeley, California 94720, United States^{||}Center of Research Excellence in Nanotechnology, King Fahd University of Petroleum and Minerals, Dhahran 34464, Saudi Arabia

Supporting Information

ABSTRACT: A presynthesized, square planar copper imidazole complex, $[\text{Cu}(\text{imidazole})_4](\text{NO}_3)_2$, was utilized as a precursor in the synthesis of a new series of zeolitic imidazolate frameworks, termed ZIF-202, -203, and -204. The structures of all three members were solved by single-crystal X-ray diffraction analysis, which revealed ZIF-203 and -204 having successfully integrated square planar units within the backbones of their respective frameworks. As a result of this unit, the structures of both ZIF-203 and -204 were found to adopt unprecedented three-dimensional nets, namely, **ntn** and **thl**, respectively. One member of this series, ZIF-204, was demonstrated to be highly porous, exhibit exceptional stability in water, and selectively capture CO_2 over CH_4 under both dry and wet conditions without any loss in performance over three cycles. Remarkably, the regeneration of ZIF-204 was performed under the mild conditions of flowing a pure N_2 gas through the material at ambient temperature.



1. INTRODUCTION

Metal–organic frameworks (MOFs) derived from imidazolate linkers are typically referred to as zeolitic imidazolate frameworks (ZIFs) or zeolite-like metal–organic frameworks (ZMOFs).^{1,2} These crystalline, extended materials have proven attractive as a result of their porosity, water stability, and even hydrophobic properties.^{2,3} Similar to MOFs, the structures of ZIFs are facilely tunable with respect to incorporating functional groups that positively influence interactions with gas molecules.^{4,5} However, thus far, functionalization of ZIF structures has primarily been limited to the linkers used to construct the frameworks^{6,7} or through employing a mixture of two linkers in the synthesis as opposed to modifying the metal clusters.^{5,8,9} The reason for this is that the majority of reported ZIFs are constructed from coordinatively saturated, tetrahedral inorganic secondary building units (SBUs).¹⁰ This is in stark contrast to the large library of inorganic SBUs used to make MOF structures, which have the readily exploited potential of endowing these materials with a greater degree of structural variety as well as enhanced properties.^{1,11} In terms of gas storage and capture applications, inorganic SBUs in MOFs, most notably those containing coordinatively unsaturated metal sites, are widely recognized as playing a key role in greatly increasing the interactions and affinity of the framework with gas molecules.^{12–14}

Inspired by the synthesis of zeolitic boron imidazolate frameworks, whereby boron imidazolate complexes were employed as precursors to form 3-connected or (3,4)-connected imidazolate frameworks,^{15,16} we imagined the possibility of introducing square planar SBUs (with coordinatively unsaturated metal sites) into structurally diverse ZIF-type materials possessing unique CO_2 capture properties. Accordingly, our strategy made use of a presynthesized, square planar $\text{Cu}(\text{II})$ complex, namely, tetrakis(imidazole)dinitrato copper(II) $[\text{Cu}(\text{HIm})_4](\text{NO}_3)_2$,¹⁷ that was, in turn, used to construct three new extended frameworks, termed ZIF-202, -203, and -204, upon reaction with Zn^{2+} . All three structures were solved by single-crystal X-ray diffraction (SXRD) analysis, which showed only two members (ZIF-203 and -204) having incorporated a square planar unit within the backbone of the framework. Interestingly, the structures of both ZIF-203 and -204 were found to be based on unprecedented topologies (**ntn** and **thl**, respectively). We further report that ZIF-204, with its high porosity and chemical stability, was capable of selectively capturing CO_2 over CH_4 even in the presence of humidity. Remarkably, this performance was retained over three cycles without degradation of the ZIF structure, and the material was

Received: April 4, 2016

Published: June 1, 2016

Table 1. Crystal Structure Data and Refinement for ZIF-202, ZIF-203, and ZIF-204

	ZIF-202	ZIF-203	ZIF-204
empirical formula	C ₁₂ H ₁₂ N ₈ Cu ₂ Zn	C ₁₅ H ₁₈ N ₁₀ O _{1.5} Cu _{1.5} Zn	C ₁₅ H ₁₅ N ₁₀ Cu _{1.5} Zn
formula weight (g mol ⁻¹)	461.81	523.08	496.06
crystal system	tetragonal	monoclinic	monoclinic
space group	<i>P</i> 4 ₂ <i>c</i>	<i>C</i> 2/ <i>c</i>	<i>P</i> 2 ₁ / <i>n</i>
<i>a</i> (Å)	10.9562(4)	23.252(5)	11.946(2)
<i>b</i> (Å)	10.9562(4)	13.098(3)	13.302(3)
<i>c</i> (Å)	6.2181(2)	20.301(7)	17.777(4)
β (deg)	90	114.099(6)	98.35(3)
<i>V</i> (Å ³)	746.41(6)	5644(3)	2794.9(10)
<i>Z</i>	2	8	4
ρ_{calcd} (g cm ⁻³)	2.050	1.569	1.374
μ (Cu <i>K</i> α) (mm ⁻¹)	5.279	2.706	2.646
<i>R</i> _{int}	0.0256	0.0647	0.0845
<i>R</i> ₁ ^a	0.0204	0.0411	0.0761
<i>wR</i> ₂ ^b	0.0589	0.0912	0.1835

^a $R_1 = \sum ||F_o| - |F_c|| / \sum |F_o|$. ^b $wR_2 = [\sum w(F_o^2 - F_c^2)^2 / w(F_o^2)]^{1/2}$ for 723 (ZIF-202), 4430 (ZIF-203), and 2322 reflections (ZIF-204), respectively, with $I > 2\sigma(I)$.

able to be regenerated easily by flowing a pure N₂ stream at room temperature.

2. EXPERIMENTAL SECTION

Materials and General Procedures. Imidazole ($\geq 99\%$ purity, HIm), copper nitrate trihydrate ($\geq 99\%$ purity, Cu(NO₃)₂·3H₂O), zinc acetate dihydrate ($\geq 98\%$ purity, Zn(OAc)₂·2H₂O), ethanol ($\geq 99.5\%$ purity), acetic acid ($\geq 99\%$ purity), and *N,N*-dimethylformamide ($\geq 99\%$ purity, DMF) were purchased from the Aldrich Chemical Co. Anhydrous methanol (99.8% extra dry, MeOH), acetonitrile (99.9% extra dry, MeCN), and tetrabutylammonium hydroxide (TBAOH; 40 wt % in water) were obtained from Acros Organics. Deionized water was prepared from a Barnstead Easypure II (17.8 M Ω ·cm⁻¹ resistivity). All of these chemicals were used without further purification. CHN elemental microanalyses (EA) and inductively coupled plasma optical emission spectrometry (ICP-OES) were performed in the Microanalytical Laboratory of the College of Chemistry at University of California-Berkeley, using a PerkinElmer 2400 series II CHNS elemental and 5300 DV analyzers, respectively. Fourier transform infrared (FT-IR) spectra were measured from KBr pellets using a Bruker Vertex 70 system. Thermogravimetric analysis (TGA) was performed using a TA Q500 thermal analysis system with the sample held in a platinum pan under a continuous airflow. Low-pressure N₂, CO₂, and CH₄ adsorption isotherms were recorded on an Autosorb iQ2 volumetric gas adsorption analyzer. Water adsorption isotherm was measured on a Belsorp Aqua3 (BEL Japan). A liquid nitrogen bath was used for the measurement at 77 K. The measurement temperatures at 288, 298, and 308 K were controlled with a water circulator. Helium was used for the estimation of dead space for gas and water adsorption measurements. Breakthrough measurements were performed in house using an L&C Science and Technology PSA-300-LC analyzer with the bed column dimensions of 14 cm × 0.635 cm. A ThermoStar GSD320 mass spectrometer was used to monitor the gaseous effluent for CO₂, CH₄, N₂, H₂O, and O₂ from the sample bed. Ultrahigh-purity N₂, CH₄, and He gases (99.999% purity) and high-purity CO₂ (99.995%) were used throughout the adsorption and breakthrough experiments (see Supporting Information, Section S1).

Synthesis of Tetrakis(imidazole)dinitrato Copper(II), [Cu(HIm)₄](NO₃)₂. The precursor, [Cu(HIm)₄](NO₃)₂, was prepared with slight modification to a previously reported procedure.¹⁷ Specifically, for bulk-scale synthesis, a solid mixture of Cu(NO₃)₂·3H₂O (7.78 g, 32.2 mmol) and imidazole (8.75 g, 129 mmol) was dissolved in a beaker containing 150 mL of ethanol. The reaction vessel was kept open to ambient atmosphere to allow for the slow evaporation of ethanol over 3 d. After evaporation, the precursor

compound was obtained as a purple, microcrystalline powder (12.9 g, 87% yield; Supporting Information, Section S2).

Single crystals of the precursor were obtained by dissolving the microcrystalline [Cu(HIm)₄](NO₃)₂ powder (0.14 g, 0.30 mmol) in an 8 mL vial containing a solvent mixture of MeCN (4 mL) and TBAOH (0.4 mL). The vial was capped and stored at room temperature for 3 d. Violet, block-shaped crystals were collected and washed with DMF (5 × 3 mL).

Synthesis of ZIF-202, Cu₂Zn(Im)₄. A mixture of Zn(OAc)₂·2H₂O (0.052 g, 0.24 mmol) and [Cu(HIm)₄](NO₃)₂ (0.092 g, 0.20 mmol) was dissolved using a solvent mixture of DMF/water/MeOH (2/1/1, v/v). The pH of the solution mixture was adjusted to ca. 5.4 by addition of acetic acid. The solution mixture was then introduced to a borosilicate glass tube. The tube was flash frozen at 77 K using a liquid N₂ bath, evacuated for 15 min to remove oxygen, and then flame-sealed to maintain a oxygen-free environment inside the tube during the reaction process. After the sealed reaction tube was heated at 85 °C for 4 d, truncated colorless crystals were obtained. The crystals were subsequently collected and washed with DMF, water, and MeOH (3 × 2 mL, each) before SXRD analysis. For the activation procedure, as-synthesized ZIF-202 was washed five times with DMF per day (5 mL each), exchanged nine times with anhydrous MeOH (5 mL each) over the course of 3 d, and then activated at 80 °C under reduced pressure (1 mTorr) for 24 h. Yield: 65% based on copper imidazole complex. EA of activated sample: Calcd for Cu₂ZnC₁₂H₁₂N₈ = Cu₂Zn(Im)₄: C, 31.28; H, 2.63; N, 24.32%. Found: C, 31.29; H, 2.54; N, 24.10%. ICP-OES of activated sample (2.0 mg of ZIF-202 in 10 mL of HNO₃ (1.68 M)): Cu, 4.531 ppm; Zn, 2.338 ppm. FT-IR (KBr, 3500–400 cm⁻¹): 3144 (w), 3112 (w), 1699 (w), 1654 (w), 1614 (m), 1486 (s), 1465 (s), 1316 (m), 1275 (m), 1236 (m), 1172 (s), 1114 (w), 1085 (vs), 985 (w), 955 (s), 846 (w), 828 (s), 766 (s), 663 (s), 645 (w).

Synthesis of ZIF-203, Cu₃Zn₂(Im)₁₀·3H₂O. A mixture of Zn(OAc)₂·2H₂O (0.052 g, 0.24 mmol) and [Cu(HIm)₄](NO₃)₂ (0.14 g, 0.30 mmol) was dissolved in 4 mL of MeCN. The pH of solution mixture was adjusted to 8.5 by addition of TBAOH. The solution mixture was then introduced to a borosilicate glass tube. The flame-sealed tube was prepared in the same way as ZIF-202, which was left at room temperature for 6 d. Several single crystals of ZIF-203 were obtained on the walls of the sealed tube and were collected for SXRD analysis. EA of activated sample: Calcd for Cu₃Zn₂C₃₀H₃₆N₂₀O₃ = Cu₃Zn₂(Im)₁₀·3H₂O: C, 34.44; H, 3.47; N, 26.78%. Found: C, 34.51; H, 3.17; N, 26.49%. FT-IR (KBr, 3500–400 cm⁻¹): 3138 (vw), 3131 (vw), 3109 (vw), 1666 (w), 1596 (w), 1492 (w), 1471 (s), 1315 (m), 1283 (w), 1237 (m), 1168 (m), 1082 (vs), 972 (w), 949 (s), 836 (s), 752 (vs), 666 (vs), 648 (w), 626 (w).

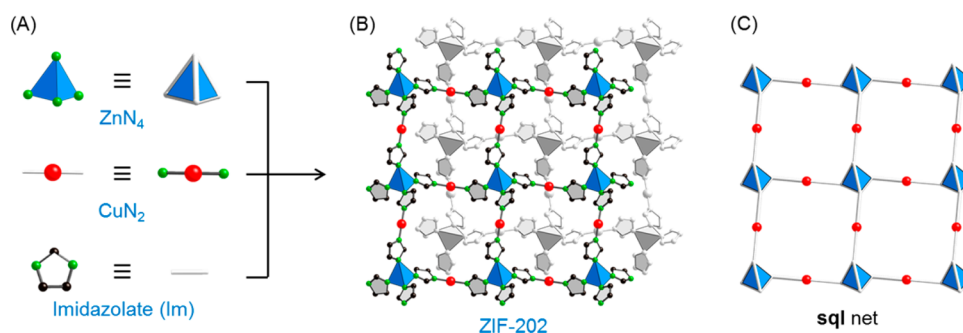


Figure 1. Single-crystal X-ray structure of ZIF-202. (A) Combining tetrahedral ZnN_4 , linear CuN_2 , and imidazole led to (B) ZIF-202. (C) The crystal structure of ZIF-202 adopts the **sql** layered topology. Atom colors: Zn, blue polyhedra; Cu, red; C, black; N, green; all H atoms are omitted for clarity.

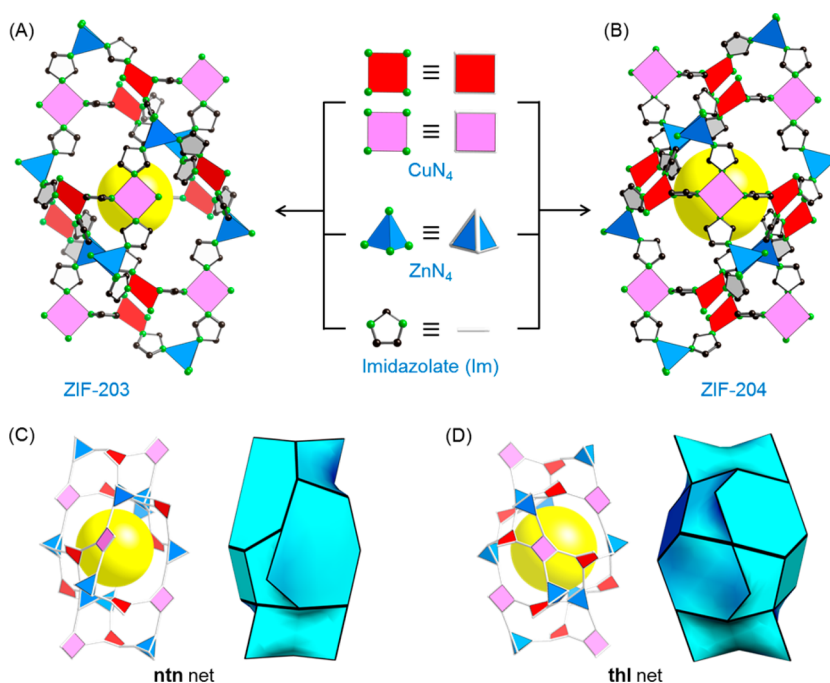


Figure 2. Single-crystal X-ray structures of ZIF-203 (A) and -204 (B) arise from combining square planar CuN_4 with tetrahedral ZnN_4 and imidazole. The structures of ZIF-203 and -204 adopt the unprecedented **ntn** (C) and **thl** topologies (D), respectively. The tiling of these new topologies are presented next to the simplified nets (C, D). Atom colors: Zn, blue polyhedra; Cu1 and Cu2, red and pink squares, respectively; C, black; N, green; all H atoms are omitted for clarity.

Synthesis of ZIF-204, $\text{Cu}_3\text{Zn}_2(\text{Im})_{10}$. A mixture of $\text{Zn}(\text{OAc})_2 \cdot 2\text{H}_2\text{O}$ (0.052 g, 0.24 mmol) and $[\text{Cu}(\text{HIm})_4](\text{NO}_3)_2$ (0.14 g, 0.31 mmol) was dissolved in a solvent mixture of DMF/water/MeCN (4/1/2, v/v). The pH of solution mixture was adjusted to 8.5 through the addition of TBAOH. The solution was then introduced to a borosilicate glass tube, and the flame-sealed tube was prepared in the same way as ZIF-203. Microcrystalline powder was obtained after allowing the sealed reaction vessel to sit for 14 d at room temperature. This powder was then collected and washed with DMF, water, and acetonitrile (3×2 mL, each). Several single crystals of ZIF-204 were obtained on the wall of the sealed tubes, which were used for SXRD analysis. For the activation procedure, as-synthesized ZIF-204 was washed five times with DMF per day (5 mL each), exchanged nine times with anhydrous MeOH over the course of 3 d (5 mL each), and then activated at 80 °C under reduced pressure (1 mTorr) for 24 h. Yield: 60% based on $\text{Zn}(\text{OAc})_2 \cdot 2\text{H}_2\text{O}$. EA of activated sample: Calcd for $\text{Cu}_3\text{Zn}_2\text{C}_{30}\text{H}_{30}\text{N}_{20} = \text{Cu}_3\text{Zn}_2(\text{Im})_{10}$: C, 36.32; H, 3.05; N, 28.23%. Found: C, 35.86; H, 2.87; N, 27.74%. ICP-OES of activated sample (5.21 mg of ZIF-204 in 10 mL of HNO_3 (1.68 M)): Cu, 10.12 ppm; Zn, 7.15 ppm. FT-IR (KBr, 3500–400 cm^{-1}): 3132 (w), 3015 (w), 2359 (w), 1758 (w), 1716 (w), 1592 (m), 1489 (w), 1474 (m), 1365

(w), 1319 (w), 1239 (m), 1217 (w), 1168 (m), 1084 (s), 974 (w), 951 (s), 836 (m), 750 (s), 666 (s), 623 (w).

3. RESULTS AND DISCUSSION

3.1. Crystal Structure Analyses of ZIF-202, -203, and -204. **ZIF-202.** SXRD analysis revealed that ZIF-202 crystallized in the tetragonal space group, $P4_2/c$ (No. 114), with unit cell parameters of $a = 10.9562(4)$ Å and $c = 6.2181(2)$ Å (Table 1; Supporting Information, Section S3). The structure of ZIF-202, formulated as $\text{Cu}_2\text{Zn}(\text{Im})_4$, can be described as a square grid of tetrahedral Zn atoms that are connected through linear $\text{Cu}(\text{Im})$ units (Figure 1). Interestingly, the square planar $[\text{Cu}(\text{HIm})_4](\text{NO}_3)_2$ precursor decomposed over the course of the reaction with Cu being reduced from Cu(II) to Cu(I). The latter is suggested as the Cu–N bond length (1.8595 Å), and resulting linear geometry is indicative of Cu(I).^{15,18} The extended, two-dimensional framework of ZIF-202 adopts the **sql** topology with staggered layers (Figure 1). Specifically, the tetrahedral Zn unit of one layer resides in the middle of square

window generated in the second layer, and the Cu units from each layer are relatively eclipsed. The center-to-center distance between two Cu atoms from neighboring layers (3.109 Å) is much greater than Cu(I)–Cu(I) bond in Cu(Im) (2.69/2.78 Å),^{7c} such that it is unlikely interlayer Cu atoms in ZIF-202 show strong cuprophilic interactions.¹⁹

ZIF-203. SXR analysis revealed that ZIF-203 crystallizes in the monoclinic space group, $C2/c$ (No. 15), with unit cell parameters of $a = 23.252(5)$ Å, $b = 13.098(3)$ Å, $c = 20.301(7)$ Å, and $\beta = 114.099(6)^\circ$ (Table 1; Supporting Information, Section S3). In analyzing the crystal structure of ZIF-203, formulated as $\text{Cu}_3\text{Zn}_2(\text{Im})_{10}\cdot 3\text{H}_2\text{O}$, there exist three independent metal nodes; specifically, one unique Zn (Zn1) and two distinct Cu atoms (Cu1 and Cu2; Figure S5). The Zn1 atom is tetrahedrally coordinated by four imidazoles, whereas both Cu1 and Cu2 atoms adopt a square pyramidal geometry with imidazoles occupying the in-plane coordination sites and a free imidazole or disordered ligand (both MeCN and imidazole partially occupy), respectively, coordinated at the axial sites (Figure S5). Although classified as square pyramidal, Cu1 and Cu2 were treated as squares for topological analysis, as the axial ligands did not play a role in the formation of the extended framework (Figure 2A). The resulting asymmetric unit, when extended into three dimensions, formed an unprecedented framework topology, termed **ntn** (Figure 2C). This new topology is characterized by one cage $[4^2.5^4.6^4.8^2]$ comprised of 14 Cu and 10 Zn vertices (the symbol $[\dots m^n \dots]$ means that there are n faces with m -membered rings).²⁰ Considering that the synthetic conditions (MeCN) employed for realizing ZIF-203 led to poor yields, we modified the solvent system to use DMF/MeCN/H₂O with the aim of obtaining a bulk quantity of ZIF-203. The resulting microcrystalline product was successfully achieved in high yield (60%) and exhibited a homogeneous morphology when examined by scanning electron microscopy (SEM; Supporting Information, Section S4). However, powder X-ray diffraction (PXRD) analysis displayed a slightly different diffraction pattern upon comparison with the simulated pattern from the SXR data of ZIF-203. This finding led to the identification of a new material, termed ZIF-204.

ZIF-204. Upon careful examination of the reaction tube, one large, transparent, and crack-free single crystal (dimensions of $0.305 \times 0.207 \times 0.202$ mm³) was found and collected for SXR analysis (Table 1 and Supporting Information, Section S3). Accordingly, ZIF-204 crystallized in the monoclinic space group, $P2_1/n$ (No. 14), with unit cell parameters of $a = 11.946(2)$ Å, $b = 13.302(3)$ Å, $c = 17.777(4)$ Å, and $\beta = 98.35(3)^\circ$ (Table 1; Supporting Information, Section S3). Similar to ZIF-203, the crystal structure of ZIF-204 displayed three independent metal nodes, specifically, one Zn (Zn1) and two Cu (Cu1 and Cu2) atoms (Figure S6). The Zn1 atom has a tetrahedral geometry, whose coordination sphere is comprised of four imidazole linkers. The Cu1 atom adopts a square pyramidal geometry with the axial site being coordinated by a DMF solvent ligand. Finally, the Cu2 atom is described as having a square planar geometry surrounded by four imidazole linkers (Figure 2B and Figure S7). When extended in three dimensions, the structure of ZIF-204 also possesses a new framework topology, named **thl** (Figure 2D). The porosity of this new architecture is derived from one cage $[4^2.5^4.6^2.7^4]$ that encompasses 14 Cu and 10 Zn vertices (Figure 2D). It is also worth noting that the PXRD pattern of the ZIF-204 bulk phase satisfactorily corresponded with that

simulated from the single crystal structure, indicating phase purity of the obtained bulk sample (Supporting Information, Sections S4 and S5). The framework topologies of ZIF-203 and -204 possess the same connectivity yet have subtle differences in terms of the connecting geometry. With the aim of highlighting these subtle differences, the structures of two compounds were rotated in different angles and were shown in Figure S7. Although the main components of both ZIF-203 and -204 are identical, the connecting angle of Zn1–Cu1–Cu2 was different (75.86° and 137.2° for ZIF-203 and -204, respectively; Figures S5–S8). This subtle difference was remarkably enough to afford two new, completely unique, three-dimensional extended structures (Figure 2).

3.2. Structural and Thermal Robustness, Permanent Porosity, and Chemical Stability. The successful synthesis of ZIF-202, -203, and -204 was proven by PXRD analysis, in which the as-synthesized diffraction pattern was in high agreement with the respective pattern calculated from the crystal structures (Supporting Information, Section S5). It is again noted that ZIF-203 was unable to be synthesized on the bulk scale, and thus it will not be further discussed. In turn, ZIF-202 and -204 were then solvent-exchanged (to remove unreacted species and noncoordinated DMF) and activated to secure fully desolvated frameworks. Structural maintenance throughout the solvent exchange and activation processes was confirmed through PXRD analysis (Supporting Information, Section S5). The color of the as-synthesized ZIF-204 sample changed from purple to dark brown after activation (Figure S15). A plausible explanation for this is that coordinatively unsaturated Cu sites were formed upon removal of axially coordinated DMF ligands under heat and reduced pressure. A similar color change was observed when the as-synthesized Cu-BTTri (where H₃BTTri = 1,3,5-tris(1H-1,2,3-triazol-5-yl)-benzene), comprised of N-donating atom-based linkers, was activated. This report also concluded that the observed color change resulted from the formation of coordinatively unsaturated Cu sites within the structure.²¹

The thermal robustness of ZIF-202 and -204 was examined by TGA, in which ZIF-202 and -204 were determined to be thermally stable up to 350 and 250 °C, respectively (Supporting Information, Section S6). There was no appreciable weight loss observed in the TGA curves up to these temperatures, indicating no presence of occluded guest molecules (i.e., both materials fully activated). Furthermore, the resulting ZnO/CuO residue for ZIF-202 and -204 was calculated to be 51.97 and 41.05%, respectively, which was in agreement with the values derived from EA (52.08 and 40.46%, respectively). The porosity of ZIF-202 and -204 was then assessed by N₂ gas adsorption analysis at 77 K (Supporting Information, Section S7). As expected, ZIF-202 revealed a nonporous material and, thus, was not considered for further study. Contrastingly, ZIF-204 exhibited a Type-I isotherm, typical of microporous materials, with BET and Langmuir surface areas of 715 and 790 m² g⁻¹, respectively (Supporting Information, Section S7).

In terms of the practical applicability of ZIF-204, chemical stability measurements were performed (Supporting Information, Section S8). Specifically, an activated sample of ZIF-204 was immersed in water, aqueous acetic acid (pH = 4.0), and aqueous sodium hydroxide (pH = 12) at room temperature for 5 d, during which each day a sample aliquot was extracted and analyzed by PXRD. Structural maintenance of ZIF-204 was proven, as the peak positions and intensities remained

unchanged under these conditions (Figures S19–S21). Moreover, the porosity of ZIF-204 was reanalyzed after the sample was suspended in water for 5 d and then reactivated. Accordingly, the N₂ isotherm at 77 K indicated a similar N₂ uptake (Figure S22). Encouraged by these results, a water adsorption isotherm was performed for ZIF-204, resulting in a Type-III profile that was highlighted by the weak interactions between water and the framework at relative pressures lower than 0.5 (Figure S23).

3.3. Gas-Adsorption Properties. Thermodynamic Uptake Capacity. Given the porosity of ZIF-204, single-component gas adsorption isotherms (CO₂ and CH₄) were investigated at 288, 298, and 308 K (Supporting Information, Section S9). Reversible isotherms were obtained for both CO₂ and CH₄ gases with ZIF-204 demonstrating significantly higher CO₂ uptake capacity (46 cm³ g⁻¹) as compared to CH₄ (13 cm³ g⁻¹) at 298 K and 800 Torr (Figure 3). It is noted that the

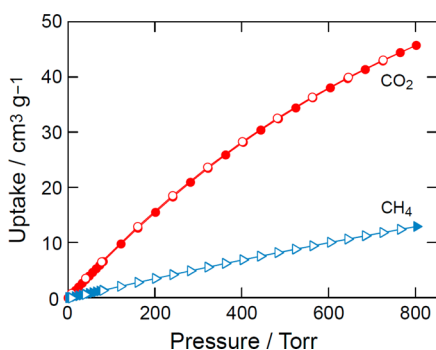


Figure 3. CO₂ (red) and CH₄ (blue) isotherms of ZIF-204 at 298 K. Filled and open symbols represent adsorption and desorption branches, respectively. The connecting lines are guides.

initial uptake in the CO₂ isotherm exhibited a steeper slope than that observed in the CH₄ isotherm at 298 K (Figure 3). This is indicative of stronger interactions (higher affinity) between the ZIF-204 framework and CO₂.

Coverage-Dependent Isosteric Enthalpy of Adsorption and Gas Selectivity. On the basis of the conclusions derived from the thermodynamic CO₂ and CH₄ uptake capacities, coverage-dependent isosteric enthalpy of adsorption (Q_{st}) for CO₂ and CH₄ were estimated using a virial-type expansion equation (Supporting Information, Section S9). It is noted that calculating Q_{st} at zero coverage will provide a quantifiable indication of the level of binding strength at the most prominent adsorptive sites within the ZIF-204 structure.^{12a,22} The initial Q_{st} value for CO₂ was found to be 29 kJ mol⁻¹, which deviates from the reported Q_{st} values for well-known, reported MOFs with coordinatively unsaturated metal sites (Mg-MOF-74, 42 kJ mol⁻¹; Cr-MIL-100, 62 kJ mol⁻¹).^{12a,13} However, this value is reminiscent of the similarly low initial Q_{st} value for Cu-BTTri (21 kJ mol⁻¹), credited to the basicity of the BTTri linker.²¹ The initial Q_{st} was also determined for CH₄ (23 kJ mol⁻¹), which was expectedly lower than the value obtained for CO₂. With these results, the CO₂/CH₄ selectivity of ZIF-204 was then estimated based on Henry's law. Accordingly, the CO₂/CH₄ selectivity of ZIF-204 was 4.6; a value that rivals other notable ZIFs, including ZIF-95 (4.3), ZIF-68 (5.0), and ZIF-70 (5.2).^{10a,23}

Dynamic CO₂ Capture via Breakthrough Measurements. Dynamic breakthrough measurements were performed to demonstrate the performance of ZIF-204 for separating CO₂

from a binary mixture containing CH₄ (Supporting Information, Section S10). Thus, a fixed bed was packed with activated ZIF-204 and subsequently subjected to a binary gas mixture containing CO₂ (35%, v/v) and CH₄ (65%, v/v) at room temperature. It is worthwhile to note that the composition of this binary gas mixture was chosen to simulate the typical volumetric percentage of CO₂ and CH₄ found in biogas sources produced from the decomposition of organic matter.²⁴ Biogas represents a viable alternative energy source (once upgraded), notably in Vietnam, which is a mass producer of large quantities of organic waste from agricultural and livestock activities. As shown in Figure 4A, ZIF-204 was effectively able to capture

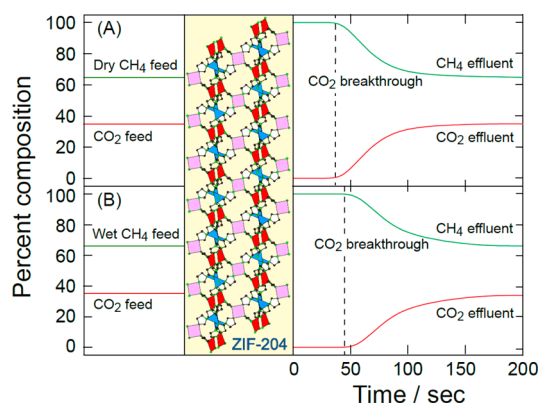


Figure 4. A binary mixture of CO₂ and dry CH₄ (A) or wet (60% relative humidity) CH₄ (B) is flown through a fixed bed of ZIF-204. The breakthrough time is indicated by the dashed line.

only CO₂ from this binary mixture, while CH₄ passed through the material unencumbered. The dynamic CO₂ uptake capacity, calculated as a result of the breakthrough time, was found to be 6.5 cm³ g⁻¹ (1.3 wt %; Table 2).

Table 2. Surface Area, Thermodynamic CO₂ Uptake, CO₂/CH₄ Selectivity, Dynamic CO₂ Uptake for ZIF-204 and BPL Carbon

materials	BET SA (m ² g ⁻¹)	CO ₂ uptake (cm ³ g ⁻¹) ^a	CH ₄ uptake (cm ³ g ⁻¹) ^a	CO ₂ /CH ₄ selectivity ^b	dynamic CO ₂ uptake (cm ³ g ⁻¹) ^c	
					dry	wet
ZIF-204	715	46	13	4.6	6.5	8.3
BPL carbon	1210	47	22	3.9	6.0	4.2

^aAt 800 Torr and 298 K. ^bCalculated from pure component isotherms by Henry's law. ^cCalculated from dynamic breakthrough experiments.

From a more practical standpoint, biogas sources contain non-negligible amounts of water, which can negatively impact the CO₂/CH₄ separation capabilities of a porous material (competitive physisorption between CO₂ and H₂O). Taking this into consideration, in conjunction with the water adsorption properties of ZIF-204, we sought to demonstrate this material's ability to dynamically separate CO₂/CH₄ in the presence of water (Supporting Information, Section S10). Prior to performing this dynamic separation measurement, ZIF-204 was exposed to a wet CH₄ stream (60% relative humidity (RH)), until water saturation was detected. At the point of saturation, a dry CO₂ stream was then introduced into the wet

CH₄ stream, and the breakthrough measurement time began. Rather surprisingly, a longer CO₂ retention time was observed when compared to the measurements performed under dry conditions (Figure 4B and Table 2). The resulting dynamic CO₂ uptake capacity of ZIF-204 for this ternary gas mixture (CO₂/CH₄/H₂O) was calculated to be 8.3 cm³ g⁻¹ (1.6 wt %). The enhanced dynamic CO₂ uptake capacity under wet conditions has been reported before for HKUST-1, which has integrated coordinatively unsaturated Cu sites within its backbone.²⁵ In the case of HKUST-1, the enhanced uptake capacity under wet conditions was attributed to increasing electrostatic interactions between CO₂ and coordinated water that occupied the coordinatively unsaturated Cu sites. Indeed, as evidenced by the water isotherm of ZIF-204 (Figure S23), water molecules were adsorbed primarily at the Cu sites at $P/P_0 \approx 0.6$. It is speculated that these adsorbed water molecules might play a critical role in creating stronger interactions with CO₂, thus resulting in higher CO₂ uptake capacity. To compare the dynamic separation results obtained for ZIF-204, we performed a comparative study using BPL carbon, which is widely used in industrial settings. Accordingly, it was found that BPL carbon exhibited slightly smaller dynamic uptake capacity than ZIF-204; however, under wet conditions, the dynamic uptake capacity was nearly half that of ZIF-204 (Figures S30 and S31).

A critical consideration for realizing a material for industrial separation applications is the recyclability and corresponding regeneration conditions necessary for recycling. Therefore, we assessed these parameters by performing three consecutive breakthrough measurements on ZIF-204. Remarkably, there was no observable loss in performance of ZIF-204 under either dry or humid conditions (60% RH; Figures S28 and S29). Furthermore, ZIF-204 could be recycled through a simple regeneration procedure of flowing a pure dry N₂ stream through the loaded bed at ambient temperature.

4. SUMMARY

The strategy of using a presynthesized square planar complex, [Cu(HIm)₄](NO₃)₂, was successful in leading to the formation of three new ZIFs. Noteworthy is the fact that this synthetic method allowed for the introduction of SBUs with new coordination modes, thus greatly expanding the possibility of structural diversity in ZIFs beyond those constructed from the conventional tetrahedral SBU units. Indeed, this strategy paves the way for producing new ZIF topologies, which will inevitably support future, detailed structure–function studies. Of the three new ZIFs reported herein, ZIF-204 was highlighted as highly porous and enhanced interactions with CO₂ over CH₄ (CO₂/CH₄ selectivity of 4.6 as calculated by Henry's law). Following this finding, dynamic breakthrough experiments were performed on ZIF-204 using a gas mixture that simulated the volumetric gas percentages found in biogas sources. The results indicated a greater dynamic CO₂ uptake capacity under wet conditions when compared to dry conditions. The breakthrough experiments were repeated up to three cycles for ZIF-204 with no structural degradation or loss in separation performance observed. Finally, ZIF-204 was easily regenerated by purging with a N₂ flow at ambient temperature.

■ ASSOCIATED CONTENT

Supporting Information

The Supporting Information is available free of charge on the ACS Publications website at DOI: 10.1021/acs.inorgchem.6b00814.

Full synthetic and characterization details of the [Cu(HIm)₄](NO₃)₂ precursor, ZIF-202, ZIF-203, and ZIF-204 (e.g., PXRD, TGA curves, SEM micrographs, and water adsorption isotherms). Gas adsorption isotherms and the experimental conditions for breakthrough measurements are provided as well. (PDF)

X-ray crystallographic information (CIF)

X-ray crystallographic information (CIF)

X-ray crystallographic information (CIF)

X-ray crystallographic information (CIF)

■ AUTHOR INFORMATION

Corresponding Authors

*E-mail: furukawa@berkeley.edu. (H.F.)

*E-mail: kcordova@berkeley.edu. (K.E.C.)

Author Contributions

#N.T.T.N. and T.N.H.L. contributed equally.

Funding

Financial support for the synthesis, characterization, and gas adsorption measurements were provided by VNU-HCM (A2015–50–01-HĐ-KHCN) and the United States Office of Naval Research Global: Naval International Cooperative Opportunities in Science and Technology Program (No. N62909–15–1N056).

Notes

The authors declare no competing financial interest.

■ ACKNOWLEDGMENTS

We thank Prof. O. M. Yaghi (UC Berkeley) for his support and mentorship throughout this project. Further, we are grateful to Dr. K. Hamada (Yaghi group) for his initial work on mixed-metal ZIFs and Mr. B. Rungtaweeveranit for his assistance with elemental analysis. We acknowledge Dr. A. T. L. Nguyen, Mr. H. L. Nguyen, and Assoc. Prof. H. T. Nguyen (VNU-HCM) for their valuable inputs. Finally, we are indebted to Prof. M. O'Keeffe (Arizona State Univ.) for helpful discussion on topological analysis. J. K. acknowledges support from the Mid-Career Researcher Program of the National Research Foundation of Korea funded by the Ministry of Science, ICT, and Future Planning (NRF-2014R1A2A1A11054190).

■ REFERENCES

- (1) (a) Eddaoudi, M.; Sava, D. F.; Eubank, J. F.; Adil, K.; Guillemin, V. *Chem. Soc. Rev.* **2015**, *44*, 228–249. (b) Furukawa, H.; Cordova, K. E.; O'Keeffe, M.; Yaghi, O. M. *Science* **2013**, *341*, 1230444.
- (2) (a) Park, K. S.; Ni, Z.; Côté, A. P.; Choi, J. Y.; Huang, R.; Uribe-Romo, F. J.; Chae, H. K.; O'Keeffe, M.; Yaghi, O. M. *Proc. Natl. Acad. Sci. U. S. A.* **2006**, *103*, 10186–10191. (b) Huang, X.-C.; Lin, Y.-Y.; Zhang, J.-P.; Chen, X.-M. *Angew. Chem., Int. Ed.* **2006**, *45*, 1557–1559.
- (3) (a) Gao, F.; Li, Y.; Bian, Z.; Hu, J.; Liu, H. *J. Mater. Chem. A* **2015**, *3*, 8091–8097. (b) Ge, D.; Lee, H. K. *J. Chromatogr. A* **2011**, *1218*, 8490–8495. (c) Ortiz, A. U.; Freitas, A. P.; Boutin, A.; Fuchs, A. H.; Coudert, F.-X. *Phys. Chem. Chem. Phys.* **2014**, *16*, 9940–9949. (d) Nguyen, N. T. T.; Furukawa, H.; Gándara, F.; Nguyen, H. T.; Cordova, K. E.; Yaghi, O. M. *Angew. Chem., Int. Ed.* **2014**, *53*, 10645–10648.

- (4) Thompson, J. A.; Brunelli, N. A.; Lively, R. P.; Johnson, J. R.; Jones, C. W.; Nair, S. J. *Phys. Chem. C* **2013**, *117*, 8198–8207.
- (5) Banerjee, R.; Furukawa, H.; Britt, D.; Knobler, C.; O’Keeffe, M.; Yaghi, O. M. *J. Am. Chem. Soc.* **2009**, *131*, 3875–3877.
- (6) (a) Nouar, F.; Eckert, J.; Eubank, J. F.; Forster, Eddaoudi, M. *J. Am. Chem. Soc.* **2009**, *131*, 2864–2870. (b) Wang, S.; Zhao, T.; Li, G.; Wojtas, L.; Huo, Q.; Eddaoudi, M.; Liu, Y. *J. Am. Chem. Soc.* **2010**, *132*, 18038–18041. (c) Zhang, S.-Y.; Shi, W.; Cheng, P.; Zaworotko, M. J. *J. Am. Chem. Soc.* **2015**, *137*, 12203–12206.
- (7) (a) Hayashi, H.; Cote, A. P.; Furukawa, H.; O’Keeffe, M.; Yaghi, O. M. *Nat. Mater.* **2007**, *6*, 501–506. (b) Wang, B.; Cote, A. P.; Furukawa, H.; O’Keeffe, M.; Yaghi, O. M. *Nature* **2008**, *453*, 207–211. (c) Zhang, J.-P.; Chen, X.-M. *Chem. Commun.* **2006**, 1689–1699. (d) Zhang, J.-P.; Zhang, Y.-B.; Lin, J.-B.; Chen, X.-M. *Chem. Rev.* **2012**, *112*, 1001–1033.
- (8) (a) Wang, F.; Tang, Y.-H.; Zhang, J. *Inorg. Chem.* **2015**, *54*, 11064–11066. (b) Wu, T.; Bu, X.; Zhang, J.; Feng, P. *Chem. Mater.* **2008**, *20*, 7377–7382.
- (9) Banerjee, R.; Phan, A.; Wang, B.; Knobler, C.; Furukawa, H.; O’Keeffe, M.; Yaghi, O. M. *Science* **2008**, *319*, 939–943.
- (10) (a) Phan, A.; Doonan, C. J.; Uribe-Romo, F. J.; Knobler, C. B.; O’Keeffe, M.; Yaghi, O. M. *Acc. Chem. Res.* **2010**, *43*, 58–67. (b) Zheng, S.-T.; Mao, C.; Lee, S.; Feng, P.; Bu, X. *J. Am. Chem. Soc.* **2012**, *134*, 11936–11939.
- (11) (a) Liu, J.; Chen, L.; Cui, H.; Zhang, J.; Zhang, L.; Su, C.-Y. *Chem. Soc. Rev.* **2014**, *43*, 6011–6061. (b) Chughtai, A. H.; Ahmad, N.; Younus, H. A.; Laypkov, A.; Verpoort, F. *Chem. Soc. Rev.* **2015**, *44*, 6804–6849.
- (12) (a) Sumida, K.; Rogow, D. L.; Mason, J. A.; McDonald, T. M.; Bloch, E. D.; Herm, Z. R.; Bae, T.-H.; Long, J. R. *Chem. Rev.* **2012**, *112*, 724–781. (b) He, Y.; Zhou, W.; Qian, G.; Chen, B. *Chem. Soc. Rev.* **2014**, *43*, 5657–5678. (c) Banerjee, D.; Cairns, A. J.; Liu, J.; Motkuri, R. K.; Nune, S. K.; Fernandez, C. A.; Krishna, R.; Strachan, D. M.; Thallapally, P. K. *Acc. Chem. Res.* **2015**, *48*, 211–219.
- (13) Llewellyn, P. L.; Bourrelly, S.; Serre, C.; Vimont, A.; Daturi, M.; Hamon, L.; De Weireld, G.; Chang, J.-S.; Hong, D.-Y.; Kyu Hwang, Y.; Hwa Jhung, S.; Férey, G. *Langmuir* **2008**, *24*, 7245–7250.
- (14) (a) Dietzel, P. D. C.; Besikiotis, V.; Blom, R. *J. Mater. Chem.* **2009**, *19*, 7362–7370. (b) Pang, J.; Jiang, F.; Wu, M.; Liu, C.; Su, K.; Lu, W.; Yuan, D.; Hong, M. *Nat. Commun.* **2015**, *6*, 7575. (c) Bae, Y.-S.; Snurr, R. Q. *Angew. Chem., Int. Ed.* **2011**, *50*, 11586–11596. (d) Lin, L.-C.; Kim, J.; Kong, X.; Scott, E.; McDonald, T. M.; Long, J. R.; Reimer, J. A.; Smit, B. *Angew. Chem., Int. Ed.* **2013**, *52*, 4410–4413. (e) Caskey, S. R.; Wong-Foy, A. G.; Matzger, A. J. *J. Am. Chem. Soc.* **2008**, *130*, 10870–10871.
- (15) Zhang, J.; Wu, T.; Zhou, C.; Chen, S.; Feng, P.; Bu, X. *Angew. Chem., Int. Ed.* **2009**, *48*, 2542–2545.
- (16) (a) Zhang, H.-X.; Liu, M.; Wen, T.; Zhang, J. *Coord. Chem. Rev.* **2016**, *307*, 255–266. (b) Lu, Z.; Knobler, C. B.; Furukawa, H.; Wang, B.; Liu, G.; Yaghi, O. M. *J. Am. Chem. Soc.* **2009**, *131*, 12532–12533. (c) Wu, T.; Zhang, J.; Zhou, C.; Wang, L.; Bu, X.; Feng, P. *J. Am. Chem. Soc.* **2009**, *131*, 6111–6113.
- (17) McFadden, D. L.; McPhail, A. T.; Gross, P. M.; Garner, C. D.; Mabbs, F. E. *J. Chem. Soc., Dalton Trans.* **1976**, 47–52.
- (18) Huang, X.-C.; Zhang, J.-P.; Lin, Y.-Y.; Yu, X.-L.; Chen, X.-M. *Chem. Commun.* **2004**, 1100–1101.
- (19) Mehrotra, P. K.; Hoffmann, R. *Inorg. Chem.* **1978**, *17*, 2187–2189.
- (20) O’Keeffe, M.; Peskov, M. A.; Ramsden, S. J.; Yaghi, O. M. *Acc. Chem. Res.* **2008**, *41*, 1782–1789.
- (21) Demessence, A.; D’Alessandro, D. M.; Foo, M. L.; Long, J. R. *J. Am. Chem. Soc.* **2009**, *131*, 8784–8786.
- (22) Czepirski, L.; Jagiello, J. *Chem. Eng. Sci.* **1989**, *44*, 797–801.
- (23) Li, J.-R.; Ma, Y.; McCarthy, M. C.; Sculley, J.; Yu, J.; Jeong, H.-K.; Balbuena, P. B.; Zhou, H.-C. *Coord. Chem. Rev.* **2011**, *255*, 1791–1823.
- (24) Olah, G. A.; Prakash, G. K. S.; Goepfert, A. *J. Am. Chem. Soc.* **2011**, *133*, 12881–12898.
- (25) Yazaydin, A. Ö.; Benin, A. I.; Faheem, S. A.; Jakubczak, P.; Low, J. J.; Willis, R. R.; Snurr, R. Q. *Chem. Mater.* **2009**, *21*, 1425–1430.